Colloid Polym Sci 275:263–273 (1997)

ORIGINAL CONTRIBUTION

H. Etori
H. Hirata
Y. Yamada
H. Okabayashi
M. Furusaka

Micelle formation of N-decanoylglycine and N-decanoyl-L-alanine oligomer potassium-salts and the micellar structure. A small-angle neutron scattering study

Received: 11 July 1996
Accepted: 11 September 1996

H. Etori · H. Hirata · Y. Yamada
Dr. H. Okabayashi (✉)
Department of Applied Chemistry
Nagoya Institute of Technology
Gokiso-cho, Showa-ku
Nagoya 466, Japan

M. Furusaka
BSF
National Laboratory
for High Energy Physics
1-1 Oho, Tsukuba-shi
Ibaraki 305, Japan

Abstract Potassium salts of N-decanoylglycine and N-decanoyl-L-alanine oligopeptides (monomer, dimer and trimer) were synthesized. For these oligomer salts in aqueous solutions, the microstructures of micelles have been investigated by small-angle neutron-scattering (SANS). In the calculation of SANS intensity data, the thickness of the hydrophilic layer was altered by changing the conformation of the oligomer moiety (helical and β-sheet structures). For micelles of the trimer salts, the helical structure models provide the best fit to the observed SANS intensity data. For micelles of the monomer- and dimer-salts, the β-sheet model provides the best fit to the observed data. For the monomer- and dimer-micelles, the aggregation number (n) is not dependent on the species of amino acid residue, implying that the decanoyl group plays a critical role in micelle formation. However, for the trimer micelles, the n value is dependent on the species of amino acid residue.

Key words Potassium N-acyl oligomers – micelles – SANS

Introduction

The sodium N-acyl sarcosinate molecule can be represented by the structural formula

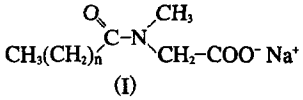

(I)

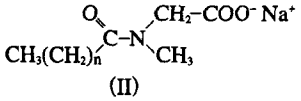

(II)

This amide molecule, as well as other simple amides, exists in both the cis (I) and trans (II) about the C–N bond of a peptide group, and the N-alkyl groups of these molecules are not magnetically equivalent due to a high energy barrier to rotation about the carbonyl carbon–nitrogen bond. Accordingly, in the NMR spectrum of this molecule, splitting of the resonance peaks of N-alkyl groups is observed. In the previous study, we have investigated the concentration dependence of the ^1H and ^{13}C NMR spectra of the sodium N-acyl sarcosinate in D_2O [1, 2]. The results can be summarized as follows.

The percentage of the trans configuration (4.6%) is less than that of the cis isomer (54%) below the critical micelle concentration (CMC). However, it increases asymptotically with further increasing concentration above the CMC, and finally approaches the constant value (76%) in the micellar state. Furthermore, incorporation of the sarcosinate anions into the sodium n-dodecyl sulfate micelles brings about an increase in the percentage of the trans isomer. These observations reveal that the trans conformation of a sarcosinate anion is more stable in the micellar state than in the monomolecular state.

Using vibrational spectroscopic methods, we have confirmed that aggregates of N-acylglycine oligopeptide

Colloid & Polymer Science, Vol. 275, No. 3 (1997)

potassium-salts and simple amides in water bring about preferential stabilization of a specific conformer [3, 4]. Beaudette et al. [5, 6] have found that a conformational change upon formation of a giant aggregate also occurs in complexes of histone proteins. Furthermore, in the lipid-membrane protein complex, we may expect that a conformational change in the protein molecule induced by the hydrophobic environment is possible, since membrane proteins can be crystallized as protein–surfactant complexes in the presence of detergent molecules [7–9] and, in fact, surfactant molecules promote the ordered packing of protein [10, 11]. However, very little is known about how the conformational change of the peptide can occur upon formation of an aggregate or incorporation into a membrane or model membrane system.

Many problems on the conformational changes of molecules still remain unresolved, and further study is needed to clarify the role of the aggregate state in the function of important biomolecules such as proteins.

In the present study, we report the detailed microstructure of micelles formed by N-decanoylglycine and N-decanoyl-L-alanine oligomer potassium salts, determined by analysis of small-angle neutron-scattering (SANS). In particular, the conformational effect of the very short oligopeptide moiety on the SANS intensity profile is discussed.

Experimental

Materials

N-decanoylglycine and N-decanoyl-L-alanine oligopeptides ($CH_3(CH_2)_8CO(NHCH_2CO)_mOH$ and $CH_3(CH_2)_8CO(NHCH(CH_3)CO)_mOH$, residue number, $m = 1, 2$ and 3) were synthesized by a stepwise procedure previously described [12, 13]. These acid type oligomers were identified by elemental analysis and the agreement between the calculated and observed values was within 0.5%. The oligomer acid types were then dissolved in methanol–water and the pH of the solution was adjusted to 7.0 by slowly adding dilute KOH–H_2O at 0 °C. The potassium salts of these oligomers were collected by lyophilization and dried under high vacuum at room temperature over P_2O_5. The monomer-, dimer- and trimer-salts (DeG_mK, $m = 1$, 2 and 3) of N-decanoylglycine oligopeptides are abbreviated as DeG1K, DeG2K and DeG3K, respectively, and those (DeA_mK, $m = 1$, 2 and 3) of N-decanoyl-L-alanine oligopeptides as DeA1K, DeA2K and DeA3K, respectively.

Molar volume determinations

The apparent molar volumes (Φ_{app}) of the decanoyl oligomer K-salts were calculated from the densities of the sample-H_2O solutions by using Eq. (1)

$$\Phi_{app} = \frac{1}{\chi}\left(\frac{1000 + \chi M}{d} - \frac{1000}{d_s}\right) \quad (1)$$

$$\Phi_{app} = \Phi^0 + A_v\chi \quad (2)$$

where χ is the molality of the solution in units of mol kg^{-1}, M is the molecular weight of the solute, d is the density of the solution, and d_s is the density of H_2O. A_v is the experimental slope and Φ^0 is the infinite dilution molar volumes of the solutes. The Φ^0 values were obtained by least-squares fitting of the Φ_{app} values to Eq. (2). The densities of the sample solutions were measured with a Lipkin–Davison type pycnometer calibrated with the known density of water. The temperature of the thermostated-bath system was controlled at 25.00 ± 0.02 °C.

Electrical conductivity measurements

The electrical conductivity method was used to determine the critical micelle concentration (CMC) from plots of the specific electrical conductivity (κ) against the oligomer K-salt concentration (C, in mol dm^{-3}). The electrical conductivities of the sample solutions were measured with Conductivity Meter CG-2A (TOA electronics Ltd.) at 25.0 ± 0.1 °C.

Neutron scattering measurements

The small-angle neutron-scattering (SANS) measurements were carried out using the medium-angle neutron-scattering instrument (WINK) installed at the pulsed neutron source KENS at the National Laboratory for High Energy Physics, Tsukuba, Japan. The sample solutions were placed in a quartz cell of 2-mm path length at 23 °C. The scattering length density (ρ) of each component was calculated using the following equation,

$$\rho = \Sigma b_i / V \quad (3)$$

where b_i is the scattering length of atom i and V is the molecular volume. The V values calculated from partial molar volume data measured in the present investigation and Σb_i values quoted from ref. [16] are listed in Table 1. The magnitude of the momentum transfer (Q) is given by Eq. (4),

$$Q = \frac{4\pi}{\lambda}\sin\left(\frac{\theta}{2}\right) \quad (4)$$

Table 1 Partial molar volumes (V) and scattering length (Σb_{coh})

species	V(Å^3)	Σb_{coh}(Å)
CH_3	42.6[a]	-4.57×10^{-5}
CH_2	28.2[a]	-8.32×10^{-6}
–ND–CH_2–CO–	60.5	2.77×10^{-4}
–ND–CH(CH_3)–CO–	89.3	2.68×10^{-4}
COO^-	25.7	1.83×10^{-4}
K^+	9.85[b]	3.71×10^{-5}

[a] ref. [14]. [b] ref. [15].

where λ is the incident wavelength (1–16 Å for WINK). The intensity of scattered neutrons was recorded on a position-sensitive 2-D detector. Normalization of the data to an absolute intensity scale was made by using the transmission of a 1 mm water sample. Corrections for the attenuation of the beam due to absorption and for multiple scattering were also made.

SANS analysis

The dependence of the neutron-scattering intensity $d\Sigma(Q)/d\Omega$ on the magnitude of a scattering vector (Q) can be expressed as a function of both the particle structure factor $P(Q)$ and the size and orientation weighted interparticle structure factor $S'(Q)$, as follows,

$$d\Sigma(Q)/d\Omega = I_0 P(Q) S'(Q) \tag{5}$$

where I_0 is the extrapolated zero-angle scattering intensity, which is independent of the micellar shape. Furthermore, I_0 is a function of the average aggregation number n and is expressed by Eq. (6) in terms of the volumes of the micelle core (V_c, in Å^3) and overall micelle (V_m, in Å^3) and the average neutron-scattering length densities of the polar shell, hydrophobic core, and solvent (ρ_p, ρ_c and ρ_s, in Å^2, respectively)

$$I_0 = \frac{(C - \mathrm{CMC})N_A}{1000\,n}\,10^{-16}[(\rho_p - \rho_c)V_c + (\rho_s - \rho_p)V_m]^2 \tag{6}$$

where N_A is Avogadro's number.

The particle structure factor $P(Q)$ for an ellipsoid particle is given by the following form,

$$P(Q) = \int_0^1 |F(Q,\mu)|^2\,d\mu \tag{7}$$

$$F(Q,\mu) = x\left(\frac{3\,(\sin(QR_1) - QR_1\cos(QR_1))}{(QR_1)^3}\right) + (1-x)\left(\frac{3\,(\sin(QR_2) - QR_2\cos(QR_2))}{(QR_2)^3}\right) \tag{8}$$

$$x = \frac{(\rho_p - \rho_c)V_c}{(\rho_p - \rho_c)V_c + (\rho_s - \rho_p)V_m} \tag{9}$$

R_1 and R_2 are given by

$$R_1 = [a^2\mu^2 + b^2(1-\mu^2)]^{1/2} \tag{10}$$

$$R_2 = [(a+t)^2\mu^2 + (b+t)^2(1-\mu)^2]^{1/2} \tag{11}$$

for the prolate model and

$$R_1 = [a^2(1-\mu^2)\mu^2 + b^2\mu^2]^{1/2} \tag{12}$$

$$R_2 = [(a+t)^2(1-\mu^2) + (b+t)^2\mu^2]^{1/2} \tag{13}$$

for the oblate model, where a and b are the major and minor axes of a micellar particle, t is the thickness of the polar core of a micellar particle, and μ is the cosine of the angle between the direction of the minor axis b and the scattering vector $\mathbf{Q}$.

The size and orientation weighted interparticle structure factor $S'(Q)$ can be calculated approximately by use of the following equation

$$S'(Q) = 1 + \beta(Q,\mu)[S(Q) - 1] \tag{14}$$

$$\beta(Q,\mu) = \frac{|\langle F(Q,\mu)\rangle^2|}{\langle |F(Q,\mu)|^2\rangle} \tag{15}$$

where $S(Q)$ is the interparticle structure factor and can be calculated by use of the model proposed by Hayter and Penfold [17, 18]. In this model, the micelle is assumed to be a rigid charged sphere of diameter σ [19, 20], interacting through a dimensionless screened Coulombic potential. The dimensionless screened Coulombic potential is calculated by using the inverse screening length of the Debye–Hückel theory, defined by the ionic strength I of the solution.

For the size-dispersed system of charged hard particles, the scattering intensity can be expressed in the following form,

$$\frac{d\Sigma(Q)}{d\Omega} = \left(\sum_{i=i_{min}}^{i_{max}} n_p(i)[(\rho_p(i) - \rho_c(i))V_c(i) + (\rho_s(i) - \rho_p(i))V_m(i)]^2 P(i,Q)\right) S'(Q) \tag{16}$$

$$n_p(i) = \frac{(C - \mathrm{CMC})d(i)N_A}{1000\,i}\,[\mathrm{cm}^{-3}] \tag{17}$$

where (i) denotes the particles having aggregation number i, and $d(i)$ is the concentration distribution function of the

Colloid & Polymer Science, Vol. 275, No. 3 (1997)

monomer. It is assumed that $d(i)$ is a Gaussian function with standard deviation (square root of mean average aggregation number) [21].

Results and discussion

In our previous papers, we have reported vibrational spectroscopic evidence for conformational changes of the anions of N-acylglycine oligomers in aqueous solution [3, 4]. Results of special relevance for this study can be summarized as follows. The infrared absorption spectra of sample solutions diluted below the CMC can be explained by the coexistence of several conformations containing the polyglycine I (PGI)-like extended form and the polyglycine II (PGII)-like helix. Above the CMC, the infrared bands arising from the PGII-like helix are intensified. This result is due to preferential stabilization of the helical structure, promoted by intermolecular association of the oligomer anions. It seems that micellization promotes an intramolecular arrangement of peptide dipoles directed along the helical axis and that this compact array of peptide dipoles strongly interacts with a CO_2^- group [22], bringing about the stability of the short helix. That is, a PGII-type array of peptide dipoles is stabilized by one charged-group effect, which has been previously demonstrated by Shoemaker et al. [23].

X-ray diffraction powder patterns and vibrational spectra of trimers and tetramers of N-acyl-L-alanine oligomer acid types with various acyl chains (acetyl, butanoyl, hexanoyl and octanoyl groups), their potassium salts and their benzyl esters have been investigated by Okabayashi et al. [13]. The results show that only a conformation similar to β-poly(L-alanine) is found for these oligomers in the solid state and that the long acyl chains induce a further β-sheet structure in the hydrogen bonding of the peptide skeleton. Furthermore, the concentration dependence of the Raman spectra of these oligomer K-salts solutions has also been studied, indicating that the helical structure similar to α-poly(L-alanine) is preferentially stabilized upon micellization and that the effect of hydration on the L-alanine residues plays a critical role in stabilization of the very short α-helical structure (to be published separately).

We have tried to measure the SANS spectra of the micellar solutions of N-acyl-L-alanine oligomer K-salts with short acyl chains (acetyl–*n*-octanoyl chains) as well as the N-acylglycine oligomer K-salts. But it was unsuccessful, since N-acyl chains are probably too short to form a micelle with large aggregation numbers, which can be detected by SANS.

In the present study, N-acylglycine- and N-acyl-L-alanine = oligomer K-salts (residue number = 1, 2 and 3) with an N-decanoyl chain were synthesized. The SANS spectra of the micellar solutions of these oligomer K-salts were measured and analyzed in order to elucidate the correlation between the secondary structure of the oligopeptide moiety and the observed SANS spectra. The CMCs and partial molar volumes of these oligomer K-salts in water were also studied to assist the SANS spectra analysis of these micellar solutions.

Critical micelle concentration and partial molar volume

For DeG_mK and DeA_mK ($m = 1$, 2 and 3) in aqueous solutions, the specific electric conductivity (κ) was measured at various concentrations. From the points of inflection in the plots of κ vs. concentration, the values of the CMC were determined, and are listed in Table 2 together with average degrees of ionization (α_{ave}) of the micelles, calculated from the slopes of the two straight lines below and above the CMC. For the two series of oligomer K-salts, the value of the CMC is found to decrease with an increase in residue number, and the values for DeG_mK are very similar to those for DeA_mK.

The free energy values (ΔG^0) of micellization per monomer [24] calculated by the use of α_{ave} and the CMCs measured in the present study are also listed in Table 2. For the two series of oligomer anions, the ΔG^0 values for micellization are not so markedly dependent on the residue number and that the differences in the ΔG^0 values between DeG_mK and DeA_mK are very small, implying that the longer hydrocarbon portion rather than the oligopeptide moiety perdominantly contributes to formation of the oligomer micelles.

For DeG_mK and DeA_mK ($m = 1$, 2 and 3) in water, the apparent molar volumes (Φ_{app}) of a solute molecule was determined at 25 °C from density measurements. Limiting partial molar volumes (Φ^0) for the solutes in water were evaluated from the apparent molar volumes. It has been

Table 2 CMC, α_{ave} and ΔG^0

	CMC (mol dm^{-3})	α_{ave}	ΔG^{0a} (kJ mol^{-1})
DeG1K	5.68×10^{-2}	0.590	−24.0
DeG2K	4.42×10^{-2}	0.591	−24.9
DeG3K	3.64×10^{-2}	0.624	−25.0
DeA1K	5.68×10^{-2}	0.615	−23.6
DeA2K	4.49×10^{-2}	0.681	−23.2
DeA3K	3.63×10^{-2}	0.736	−22.9

[a] $\Delta G^0 \approx RT(2 - \alpha_{ave}) \ln X_{CMC}$.

Table 3 The infinite dilution molar volumes (Φ^0, $cm^3\ mol^{-1}$) and the partial molar volumes (Φ_a, $cm^3\ mol^{-1}$) of the micellar oligomer K-salts, for the series of DeG_mK and DeA_mK

	Φ^0 ($cm^3\ mol^{-1}$)	Φ_a ($cm^3\ mol^{-1}$)
DeG1K	208.7	219.6
DeG2K	242.7	256.8
DeG3K	277.8	292.5
DeA1K	223.9	235.9
DeA2K	279.2	290.2
DeA3K	332.9	343.4

found that the Φ_{app} values are almost constant below the CMCs for these oligomer series, while they increase linearly with an increase in concentration. Above the CMC, the Φ value is expressed by Eq. (18)

$$\Phi = \frac{CMC}{C}\Phi^0 + \frac{C - CMC}{C}\Phi_a \qquad (18)$$

where Φ_a denotes the partial molar volume of the decanoyl oligomer anion in the micellar state. The Φ^0 and Φ_a values thus obtained are listed in Table 3.

Carmel et al. [25] have measured the apparent molar volumes of glycine- and L-alanine-oligomers in water. The results provide evidence for interference of the ionic end groups of the peptides upon the hydration of the middle portion and side chains of the oligomers. In fact, contributions of segmental motions or conformational changes to the Φ value cannot be ignored, since a conformational change of both hydrocarbon and peptide moieties occurs upon micellization [1, 4, 26, 27]. The differences between the Φ^0 and Φ_a values, as can be seen in Table 3, are ascribed to the contributions of segmental mobility or conformational changes upon micellization for both the hydrocarbon portion and oligopeptide moiety.

For the two series of decanoyl oligomers in H_2O, the Φ^0 and Φ_a values depend on the residue number and provides the linear relationship between the Φ^0 and Φ_a values and the residue number (m) ($\Phi^0 = A + Bm$, $A = 173.9$: $B = 34.5$ and $A = 169.7$, $B = 54.5$ for DeG_mK and DeA_mK in monomer state, respectively; $\Phi_a = A_a + B_a m$, $A_a = 183.5$, $B_a = 36.4$ and $A_a = 182.3$, $B_a = 53.8$ for DeG_mK and DeA_mK in micellar state, respectively). The limiting partial molar volume of 182.9 $cm^3\ mol^{-1}$ for the decanoyl and carboxylate anion moieties in the micellar state is evaluated by extrapolation to the intercept. The partial molar volume data thus obtained are used in SANS analysis.

SANS spectra and micellar structure

For the micelles formed by the oligopeptide K-salts, both prolate and oblate spheroid models have been calculated by assuming both monodispersity and polydispersity.

A structural model of an oligopeptide micelle, used in the calculation of the single particle form factor $P(Q)$, is shown in Fig. 1 only for the prolate model. This model is based on the results of the SANS analysis for n-alkyltrimethylammonium bromide micelles made by Berr [24].

The shape of an oligopeptide micelle is prolate and has a hydrophobic core with a major axis a and minor axis b. The b value is set equal to the length of a portion of the fully extended n-decanoyl chain which constitutes the hydrophobic core. The hydrophilic layer, of thickness t, consists of head groups including oligopeptide moieties and carboxylate anions, associated with potassium ions and water molecules, and the hydrated methylene groups of the n-decanoyl chain.

Fig. 1 Prolate micellar model used in the calculation of $P(Q)$ and a step model of average neutron-scattering length densities. t is the thickness of the hydrophilic (Stern) layer, a and b are the major and minor axes, respectively. ρ_p, ρ_c and ρ_s are the average neutron-scattering length densities of the polar shell, hydrophobic core and solvent, respectively

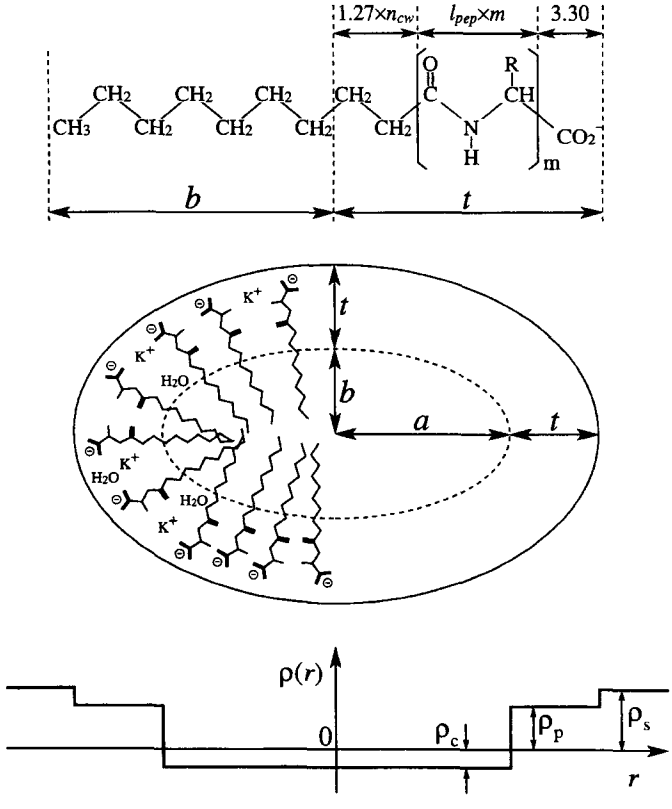

The b and t values are given by the following equations, which are similar to the equation presented by Tanford [28],

$$b = 1.50 + 1.27(9 - n_{cw}) \quad (19)$$

$$t = 1.27 \times n_{cw} + l_{pep} \times n_{pep} + 3.30 \quad (20)$$

where n_{cw} is the number of hydrated methylenes of an n-decanoyl chain, l_{pep} is the length of an oligopeptide chain (–CO–ND–CHR–; R = H and R = CH_3 for a glycine residue and for an L-alanine residue, respectively) along the molecular axis including an n-decanoyl chain, and n_{pep} is the number of peptide residues. The l_{pep} values are 3.45 Å for a β-type structure and 1.49 Å for a helical one, which were obtained from geometrical dimensions of β-sheet [29] and helical [30] structures for polypeptides, determined by x-ray diffraction analysis. The number 9 is the sum of the number of methyl carbon atoms and that of methylene carbon atoms in the n-decanoyl chain. The number 3.30 is the length of a terminal COO^- group, which was calculated using both geometrical dimensions of a COO^- group and van der Waals radius of oxygen atoms [31].

The volume of the hydrocarbon moiety constituting the core (V_{tail}) and that of the polar heads in the hydrophilic layer (V_{head}) per one oligopeptide anion, used for calculation of the scattering length densities of the whole micelle, are expressed as follows

$$V_{tail} = V_{CH_3} + (8 - n_{cw}) \times V_{CH_2} \quad (21)$$

$$V_{head} = n_{cw} \times V_{CH_2} + n_{pep} \times V_{pep} + V_{COO^-} \quad (22)$$

where V_{CH_3}, V_{CH_2}, V_{pep} and V_{COO^-} are the volumes of the methyl, methylene, peptide and carboxylate anion group, respectively. These values were calculated using partial molar volume data [14, 15] listed in Table 1.

In the SANS analysis, the scattering intensity arising from the oligopeptide K-salts solution was corrected for the detector background and incoherent scattering. The intensity spectrum of an oligopeptide solution measured at concentrations below the CMC was subtracted from those of the micellar solutions containing the oligomer K-salts in the Q range 0.06–0.30 $Å^{-1}$.

The thickness of the hydrophilic layer (t) was varied by changing a conformation of the oligopeptide moiety, which alters the SANS intensity profiles. For the conformations of the oligopeptide moiety, both PGII-type (or α-helix) and β-sheet structure models were assumed for the oligopeptide moieties of DeG3K and DeA3K.

For DeG3K and DeA3K, we have found that the helical structural model of peptide moiety provides better fit to the SANS intensity data than the β-sheet structure does, while, for DeG1K, DeG2K, DeA1K and DeA2K, the β-sheet structural model provides a better fit than the helical structure does.

In general, when the concentration of a surfactant molecule is very low and the intermicellar interaction is neglected, the SANS intensity spectrum is dominated by the particle structure factor $P(Q)$, and the interparticle structure factor $S'(Q)$ is unity throughout the observed Q range. However, when the interaction cannot be neglected as the concentration increases, $S'(Q)$ deviates from unity and the interaction peak appears in the SANS spectrum.

The SANS intensity spectra calculated by assuming monodispersity for the micellar solutions of DeG_mK and DeA_mK are shown in Fig. 2. In the curves of $I(Q)$ against Q observed in the concentration range 2.0–5.0 wt%, very broad peaks are observed, showing that there are interactions between the micelles. Moreover, as the concentration increases the interaction peak increases steadily in intensity and shifts to higher Q values, indicating an enhanced interparticle structure factor with an increase in micellar concentration.

The observed intensity data were analyzed with the aggregation number (n), degree of ionization of a micelle (α), and number of hydrated methylene groups (n_{cw}) as fitting parameters, and the a, b, and t values are calculated using n_{cw} and n. The values of extracted parameters are listed in Table 4A and 4B. The best fit scattering intensity profiles for the two series of samples are also shown in Fig. 2. The closeness of fit between the observed and calculated data is excellent. The average percentage deviation per one datum point was within ± 2–4% for all spectra.

It can be seen in Table 4 that the $(a + t)/(b + t)$ ratio of prolate spherical micelle decreases as the concentration approaches the CMC. This result indicates that the shape of an oligomer micelle changes with an increase in micellar concentration. For a micelle with a minimum aggregation number n_0, $(a + t)/(b + t)$ ratio (0.9–1.1) is very close to 1.0, showing that the minimum micelle may be spherical. Thus, we may assume for formation of the oligomer micelles that both micellar growth and sphere to prolate shape variation occur with an increase in micellar concentration, although the variation is not large.

For a series of DeG_mK, as the number of glycine residue increases, the aggregation number (n) tends to increase, as can be seen in Table 4A. Moreover, it is evident that the number of hydrated methylene groups in the hydrophilic layer decreases with an increase in the residue number, implying that the DeG_mK micelles become drier with an increase in glycine residue number. That is, we may assume that the helical structure of the glycine oligomer moieties results in a thinner hydrophilic

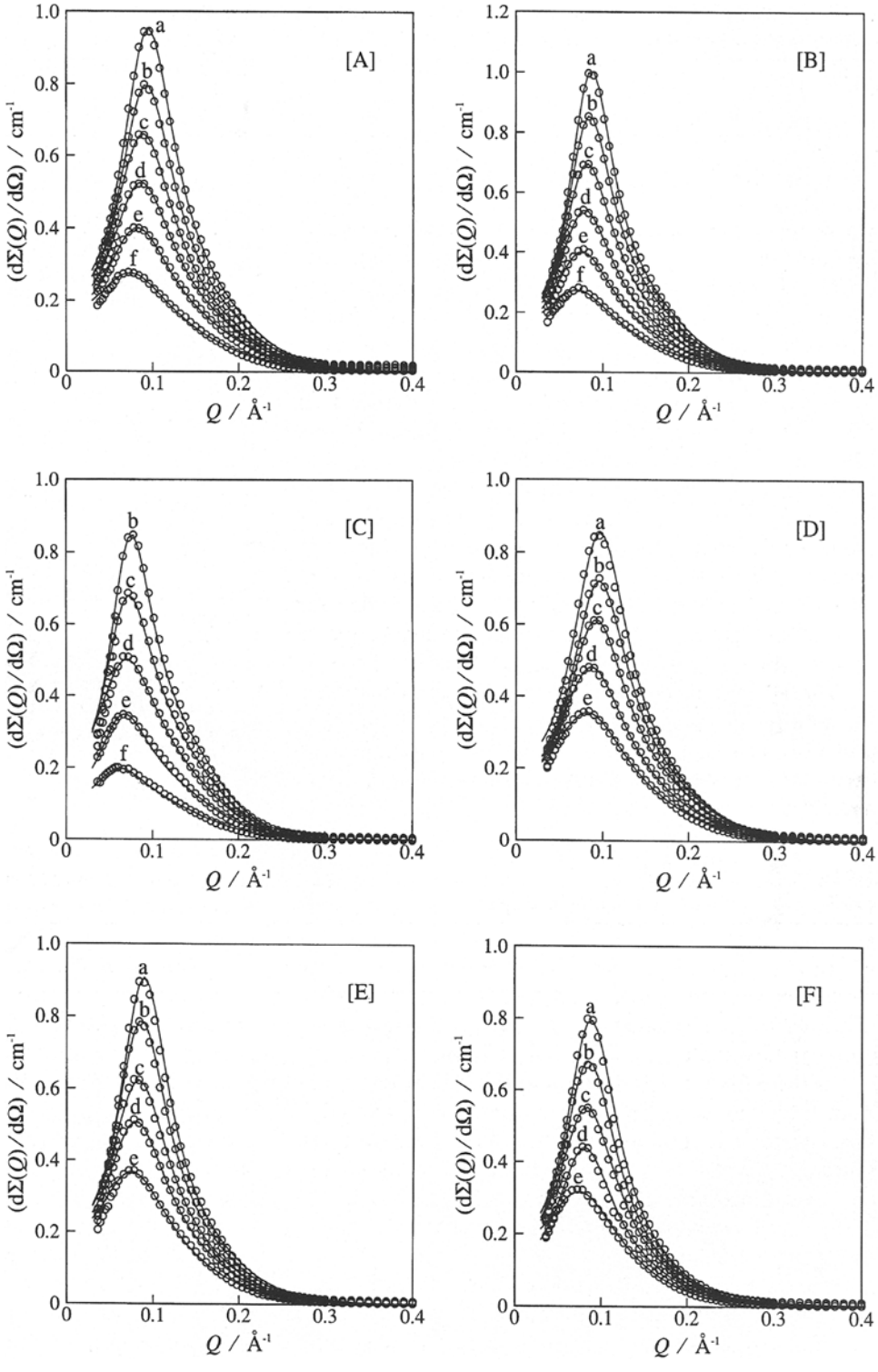

Fig. 2 Observed scattering intensity spectra (open circles) for DeG1K–D_2O [A], DeG2K–D_2O [B], DeG3K–D_2O [C], DeA1K–D_2O [D], DeA2K–D_2O [E], DeA3K–D_2O [F] systems at 23 °C: a) 5.0 wt%; b) 4.5 wt%; c) 4.0 wt%; d) 3.5 wt%; e) 3.0 wt%; f) 2.5 wt%; (solid lines) fitting scattered intensity profiles for the prolate model

Colloid & Polymer Science, Vol. 275, No. 3 (1997)

Table 4A Scattering intensity spectra observed for N-decanoylglycine oligomer K-salts micellar solutions and theoretically calculated results for prolate model (assumed monodispersity)[a]

wt%	n	α	n_{cw}	a (Å)	b (Å)	t (Å)	$\frac{(a+t)}{(b+t)}$	N_s	$1/\kappa$ (Å)	σ (Å)	Δ (%)
DeG1K–D_2O system at 23 °C											
2.5	35.3 ± 0.8	0.43 ± 0.09	2.0 ± 0 2	16.5	10.4	9.3	1.32	27.4	11.8	43.1	2.8
3.0	35.5 ± 0.7	0.40 ± 0.06	1.6 ± 0.2	15.9	10.9	8.8	1.26	25.4	11.5	42.5	2.6
3.5	36.5 ± 0.5	0.39 ± 0.04	1.7 ± 0.2	16.5	10.8	8.9	1.29	25.5	11.2	42.9	2.1
4.0	38.8 ± 0.7	0.37 ± 0.03	2.0 ± 0.2	18.2	10.4	9.3	1.40	26.1	11.0	44.0	2.4
4.5	39.6 ± 0.6	0.39 ± 0.03	2.0 ± 0.1	18.5	10.4	9.3	1.41	25.8	10.6	44.2	2.1
5.0	41.3 ± 0 6	0.38 ± 0.02	1.9 ± 0.1	19.1	10.5	9.2	1.44	24.9	10.4	44.4	2.1
DeG2K–D_2O system at 23 °C											
2.5	35.3 ± 1.1	0.41 ± 0.12	1.5 ± 0.2	15.7	11.0	12.1	1.20	44.4	13.3	49.2	3.9
3.0	37.3 ± 1.2	0.35 ± 0.12	1.5 ± 0.2	16.5	11.0	12.1	1.24	43.1	13.0	49.7	4.0
3.5	39.2 ± 1.0	0.36 ± 0.07	1.5 ± 0.2	17.4	11.0	12.1	1.28	41.9	12.7	50.2	3.7
4.0	41.2 ± 1.0	0.37 ± 0.06	1.4 ± 0.2	18.1	11.2	12.0	1.30	40.2	12.3	50.5	3.5
4.5	42.6 ± 1.0	0.38 ± 0.05	1.3 ± 0.2	18.5	11.3	11.9	1.31	38.9	11.9	50.7	3.7
5.0	44.3 ± 0.9	0.37 ± 0.04	1.4 ± 0.2	19.4	11.2	12.0	1.36	38.7	11.7	51.2	3.3
DeG3K–D_2O system at 23 °C											
2.0	40.8 ± 0.9	0.43 ± 0.08	0.9 ± 0.2	17.0	11.8	8.9	1.25	21.9	15.0	44.6	2.5
2.5	42.9 ± 1.2	0.45 ± 0.09	0.7 ± 0.2	17.6	12.0	8.7	1.27	20.4	14.4	44.8	3.0
3.0	44.7 ± 0.9	0.48 ± 0.08	0.3 ± 0.2	17.6	12.5	8.2	1.24	18.3	13.7	44.5	2.6
3.5	46.9 ± 1.4	0.52 ± 0.13	0.5 ± 0.3	18.8	12.3	8.4	1.32	18.6	13.2	45.4	3.9
4.0	48.0 ± 1.3	0.54 ± 0.11	0.7 ± 0.2	19.6	12.0	8.7	1.37	19.1	12.6	45.9	3.9

[a] n: The average aggregation number of a micelle. α: The degree of ionization of a micelle. In the present SANS analysis, it was assumed that the micellar solution is a one-component macrofluid and the finite size of the counterion is ignored. Therefore, the α values listed are an apparent charge [32]. n_{cw}: The number of hydrated methylene groups in the hydrophilic layer. a: The major axis of a prolate micelle given by $a = (3nV_{tail})/(4\pi b^2)$. b: The minor axis of a prolate micelle given by Eq. (19). t: The thickness of the hydrophilic layer given by Eq. (20). N_s: The number of water molecules associated with an oligopeptide anion. $1/\kappa$: The inverse Debye–Hückel screening length. σ: The macroion diameter. Δ: the average percentage deviation per data point. $\Delta = 100 \times [\Sigma((I_{obs} - I_{calc})/I_{calc})^2]^{1/2}$, where I_{obs} and I_{calc} denote the observed and calculated neutron-scattering intensities, respectively [33].

Table 4B Scattering intensity spectra observed for N-decanoyl-L-alanine oligomer K-salts micellar solutions and theoretically calculated results for prolate model (assumed monodispersity)[a]

wt%	n	α	n_{cw}	a (Å)	b (Å)	t (Å)	$\frac{(a+t)}{(b+t)}$	N_s	$1/\kappa$ (Å)	σ (Å)	Δ (%)
DeA1K–D_2O system at 23 °C											
3.0	30.3 ± 0.5	0.43 ± 0.06	2.2 ± 0.2	14.5	10.1	9.5	1.22	29.8	11.5	42.1	2.3
3.5	31.7 ± 0.5	0.41 ± 0.04	2.3 ± 0.2	15.4	10.0	9.7	1.27	29.5	11.2	42.6	2.1
4.0	31.7 ± 0.4	0.48 ± 0.04	2.0 ± 0.2	14.8	10.4	9.3	1.23	28.0	10.7	42.1	2.0
4.5	32.3 ± 0.5	0.46 ± 0.03	2.2 ± 0.2	15.5	10.1	9.5	1.27	28.7	10.5	42.6	2.2
5.0	34.9 ± 0.7	0.40 ± 0.03	2.4 ± 0.2	17.1	9.9	9.8	1.37	28.5	10.4	43.7	3.0
DeA2K–D_2O system at 23 °C											
3.0	30.0 ± 0.8	0.44 ± 0.09	1.5 ± 0.2	13.3	11.0	12.1	1.10	47.0	12.9	47.7	3.5
3.5	32.1 ± 0.7	0.38 ± 0.07	1.5 ± 0.2	14.2	11.0	12.1	1.14	45.1	12.7	48.3	3.4
4.0	32.9 ± 0.7	0.37 ± 0.05	1.7 ± 0.2	14.9	10.8	12.4	1.18	45.7	12.4	48.9	3.1
4.5	34.6 ± 0.7	0.40 ± 0.04	1.6 ± 0.2	15.5	10.9	12.2	1.20	43.7	12.0	49.2	3.2
5.0	35.0 ± 0.7	0.40 ± 0.04	1.7 ± 0.2	15.9	10.8	12.4	1.22	44.0	11.7	49.4	3.2
DeA3K–D_2O system at 23 °C											
3.0	24.9 ± 0.4	0.46 ± 0.06	2.9 ± 0.1	13.0	9.2	11.5	1.18	39.5	14.2	43.7	2.2
3.5	25.9 ± 0.6	0.58 ± 0.08	3.0 ± 0.1	13.6	9.1	11.6	1.22	39.2	13.3	44.2	3.2
4.0	27.8 ± 0.5	0.47 ± 0.05	3.0 ± 0.1	14.7	9.1	11.6	1.27	37.3	13.3	44.8	2.3
4.5	29.3 ± 0.6	0.49 ± 0.05	3.1 ± 0.2	15.6	9.0	11.7	1.32	36.7	12.8	45.4	3.0
5.0	30.2 ± 0.7	0.48 ± 0.05	3.1 ± 0.1	16.1	9.0	11.7	1.34	36.0	12.5	45.7	3.4

layer and makes smaller the depth of water penetration into the hydrocarbon core.

For a series of DeA_mK, it is found that the dependence of the n value on the residue number is very small. In fact, the n values of the DeG3K micelles are smaller than those for DeA1K and DeA2K micelles. We may note the increased number of hydrated methylene groups for DeA3K micelles, implying that the DeA3K micelles becomes wetter compared with the DeA1K and DeA2K micelles.

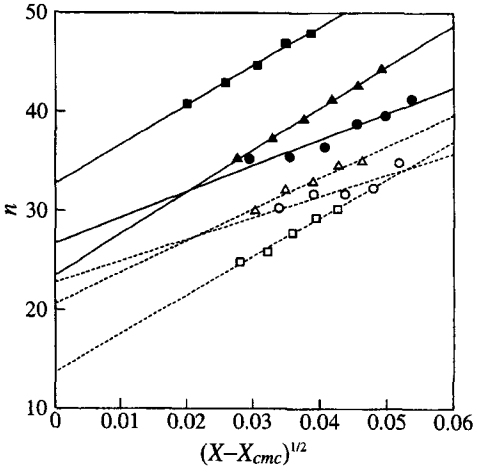

Fig. 3 Plot of aggregation number (n) as a function of the square root of the monomer concentration-forming-micelles (X = molar fraction): (●) DeG1K; (▲) DeG2K; (■) DeG3K; (○) DeA1K; (△) DeA2K; (□) DeA3K

Figure 3 shows the average aggregation number n plotted against $(X - X_{CMC})^{1/2}$, which is a square root of the monomer concentration attributable to formation of micelles expressed by molar fraction [34]. For all micellar solutions of DeG_mK and DeA_mK, the n values increase with an increase in micellar concentration, and all the n values fall on a straight line. Therefore, a ladder model of micellar growth, which has been proposed by Missel et al. [34], can also be applied to the micellar formation of these oligopeptide K-salts.

Extrapolation of the straight line n vs. $(X - X_{CMC})^{1/2}$ gives the minimum aggregation number (n_0) of a micelle at the CMC: the n_0 values of DeG_mK are 26.7, 23.5 and 32.8 for $m = 1$, 2 and 3, respectively, and those of DeA_mK are 22.8, 20.6 and 13.7 for $m = 1$, 2 and 3, respectively. When we compare the n_0 values for these oligopeptide monomer- and dimer-salts, it is found that these values are not dependent on the residue number, implying that the hydrocarbon moiety for these short oligomer K-salts contributes predominantly to formation of a minimum micelle. However, for the micelles of DeG3K and DeA3K anions, it is evident that there exists the significant difference between the n_0 values.

For the oblate spheroid model of the DeG_mK and DeA_mK micellar systems, the observed intensity data were

Table 5 Scattering intensity spectra observed for N-decanoylglycine and N-decanoyl-L-alanine oligomer K-salts micellar solutions and theoretically calculated results for oblate model (assumed monodispersity)[a]

wt%	n	α	n_{cw}	a (Å)	b (Å)	t (Å)	$\frac{(a+t)}{(b+t)}$	N_s	$1/\kappa$ (Å)	σ (Å)	Δ (%)
DeG1K–D_2O system at 23 °C											
2.5	35.3 ± 0.7	0.43 ± 0.08	2.3 ± 0.2	13.1	10.0	9.7	1.16	28.1	12.1	43.4	2.5
5.0	41.0 ± 0.5	0.37 ± 0.02	2.4 ± 0.2	14.1	9.9	9.8	1.21	26.1	10.5	44.8	2 1
DeG2K–D_2O system at 23 °C											
2.5	35.4 ± 1.0	0.41 ± 0.11	1.7 ± 0.2	13.1	10.8	12.4	1.10	45 0	13.3	49.4	3.7
5.0	44.2 ± 0.8	0.37 ± 0.03	1.8 ± 0.2	14.7	10.6	12.5	1.17	39.6	11.7	51.5	2.9
DeG3K–D_2O system at 23 °C											
2.0	40.8 ± 0.7	0.43 ± 0.07	1.2 ± 0.2	14.1	11.4	9.3	1.13	22.7	15.0	45.0	2.2
4.0	48.2 ± 0.9	0.44 ± 0.09	1.2 ± 0.2	15.4	11.4	9.3	1.19	20.3	13.1	46.5	3.0
DeA1K–D_2O system at 23 °C											
3.0	30.3 ± 0.4	0.43 ± 0.05	2.4 ± 0.2	12.1	9.9	9.8	1.11	30.4	11.5	42.3	2.1
5.0	34.7 ± 0.7	0.39 ± 0.03	2.8 ± 0.2	12.9	9.4	10.3	1.18	29.6	10.5	44.0	3.3
DeA2K–D_2O system at 23 °C											
3.0	30.1 ± 0.7	0.45 ± 0.09	1.6 ± 0.2	12.1	10.9	12.2	1.05	47.4	12.9	47.9	3.4
5.0	35.0 ± 0 7	0.40 ± 0.04	1.9 ± 0.2	13.1	10.5	12.6	1.11	44.6	11.7	49.6	3.2
DeA3K–D_2O system at 23 °C											
3.0	24.9 ± 0.4	0.46 ± 0.07	3.0 ± 0.1	10.9	9.1	11.6	1.09	39.7	14.2	43.8	2.2
5.0	29.9 ± 0.7	0.48 ± 0.05	3.3 ± 0.2	12.0	8.7	12.0	1.16	36.2	12.5	45.6	4.0

[a] a: The major axis of an oblate micelle given by $a = \{(3nV_{tail})/(4\pi b)\}^{1/2}$. b: The minor axis of an oblate micelle given by Eq. (19).

Colloid & Polymer Science, Vol. 275, No. 3 (1997)

Table 6 Observed scattering intensity spectra for the representative N-decanoyl oligomer K-salts micellar solutions and theoretically calculated results for prolate model (assumed polydispersity)

	n_{ave}	α	n_{cw}	Δ(%)
DeG1K–D_2O 5.0 wt%	42	0.38	1.8	2.3
DeA1K–D_2O 5.0 wt%	35	0.39	2.4	3.2

analyzed with the same fitting parameters (n, α and n_{cw}). The best fit scattering intensity profiles for the two series of samples (error: $\pm$ 2–4%) were obtained (profiles not shown). The values of extracted parameters were in good agreement with those calculated by the prolate model, and are listed in Table 5 only for the representative samples. The n values vs. $(X - X_{CMC})^{1/2}$ plots were in accord with those for the prolate model.

Thus, we may assume that the micellar shape of the DeG_mK and DeA_mK systems is a prolate or oblate spheroid. However, when we consider the packing parameters of these surfactant molecules, the prolate model seems to be much better than the oblate model, since the packing parameters of both the DeG_mK and DeA_mK surfactants are in the range 0.25–0.36.

We may discuss the relationship between the molecular packing parameters of a surfactant and micellar shape. For surfactant molecules of optimal area a_0, hydrocarbon volume V, and critical chain length l_c, the packing parameter is defined as V/a_0l_c. As has been shown by Israelachvili [21], we may expect that surfactant molecules form prolate micelles at $V/a_0l_c < 1/2$, and oblate micelles at $V/a_0l_c > 1/2$. Therefore, for the two surfactant series used in the present study, we may expect that both the DeG_mK and DeA_mK systems form prolate micelles.

In the present study, the scattering intensity $(d\Sigma(Q)/d\Omega)$ was also calculated by considering the polydispersity (Eqs. (16) and (17)) and use was also made of the interparticle structure factor $S'(Q)$. The calculated $d\Sigma(Q)/d\Omega$ profiles are not shown here. It has been found that the calculated average aggregation number (n_{ave}) values are very similar to aggregation number calculated by assuming monodispersity. The results for the representative sample solutions are listed in Table 6.

Conclusion

For the N-acylglycine and N-acly-L-alanine oligomer K-salts-D_2O solutions, SANS spectra have been measured at various concentrations. In the SANS intensity spectra, very broad peaks were observed, showing that there are interactions between the micelles. Moreover, it was found that an interparticle structure factor is enhanced with an increase in micellar concentration.

Both prolate and oblate spheroid models, for the micelles formed by the N-acyl oligopeptide K-salts in water, have been calculated by assuming monodispersity. Both the prolate and oblate models have been found to provide the best fits to the SANS intensity data. However, we suggest that the micellar shape of the two surfactant systems may be a prolate, considering the packing parameters.

In the calculation, the thickness of the hydrophilic layer was altered by changing a conformation of the oligomer moiety (helical and β-sheet conformations). For K-salts of the glycine and L-alanine monomers and dimers, the β-sheet structural model provides a better fit than the helical structure does. For the trimer salts, however, the helical structural models provide a better fit to the SANS intensity data than β-sheet structure does. Thus, the conformation of an oligopeptide moiety affects the SANS intensity profile.

In the concentration range 3.0–5.0 wt%, for the micelles of the oligomer, monomer, and dimer anions, the micellar shape and the aggregation number are not so dependent on the species of amino acid residue, implying that the decanoyl group contributes predominantly to micellization. However, for the micelles of the trimer K-salts, it is evident that the aggregation number depends on a species of amino acid residue in the concentration range measured. The scattering intensity was also calculated by considering the polydispersity. The calculated average aggregation number values were in good agreement with those estimated by assuming the monodispersity.

Thus, the SANS results of N-acyl oligomer K-salts in the micellar state, provide fundamental data in order to understand the SANS intensity spectra of surfactant-protein complexes. However, SANS experiments for N-acyl oligopeptides with higher residue number or with various species of amino acid are highly desirable.

References

1. Takahashi H, Nakayama Y, Hori H, Kihara K, Okabayashi H, Okuyama M (1976) J Colloid Interface Sci 54:102–107
2. Okabayashi H, Yoshida T, Terada Y, Matsushita K (1982) J Colloid Interface Sci 87:527–536
3. Okabayashi H, Ohshima K, Etori H, Taga K, Yoshida T, Nishio E (1989) J Phys Chem 93:6638–6642

4. Okabayashi H, Taga K, Yoshida T, Ohshima K, Etori H, Uehara T, Nishio E (1991) Appl Spectrosc 45: 626–631
5 Beaudette NV, Fulmer AW, Okabayashi H, Fasman GD (1981) Biochemistry 20:6526–6535
6. Beaudette NV, Okabayashi H, Fasman GD (1982) Biochemistry 21:1765–1772
7. Michel H, Oesterhelt D (1980) Proc Natl Acad Sci USA 77:1283–1285
8. Garavito RM, Rosenbusch JP (1980) J Cell Biol 86:327–329
9. Michel H (1982) J Mol Biol 158:567–572
10. Michel H (1983) Trends Biochem Sci 8:56–59
11. Garavito RM, Markovic-Housley Z, Jenkins JA (1986) J Cryst Growth 76:701–709
12. Okabayashi H, Ohshima K, Etori H, Debnath R, Taga K, Yoshida T, Nishio E (1990) J Chem Soc Faraday Trans 86:1561–1567
13. Okabayashi H, Etori H, Yamada Y, Taga K, Yoshida T (1996) Vib Spectrosc: in press
14. Vaas S, Török T, Jákli G, Berecz E (1989) J Phys Chem 93:6553–6559
15. Marcus Y (1983) J Solution Chem 12: 271–275
16 Sears VF (1986) In: Sköld K, Price DL (eds) Methods of Experimental Physics. Vol 23 part A, Academic Press, Orlando, pp 521–550
17. Hayter JB, Penfold J (1981) Mol Phys 42:109–118
18. Hansen JP, Hayter JB (1982) Mol Phys 46:651–656
19. Kotlarchyk M, Chen SH (1983) J Chem Phys 79:2461–2469
20 Chen SH, Lin TL (1987) In: Price DL, Sköld K (eds) Methods of Experimental Physics. Vol. 23 Part B, Academic Press, San Diego, pp 489–543
21. Israelachvili JN (1992) In: Intermolecular and Surface Forces. Academic Press, London, pp 341–394
22 Blagdon DE, Goodman M (1975) Biopolymers 14:241–245
23. Shoemaker KR, Kim PS, York EJ, Stewart JM, Baldwin RL (1987) Nature (London) 326:563–567
24. Berr SS (1987) J Phys Chem 91: 4760–4765
25. Carmel J, Boileau J (1978) Can J Chem 56:2707–2713
26. Okabayashi H, Okuyama M, Kitagawa T (1975) Bull Chem Soc Jpn 48: 2264–2269
27. Okabayashi H, Taga K, Tsukamoto K, Tamaoki H, Yoshida T, Matsuura H (1985) Chemica Scripta 25:153–156
28. Tanford C (1972) J Phys Chem 76: 3020–3024
29. Arnott S, Dover SD, Elliott A (1967) J Mol Biol 30:201–208
30. Arnott S, Wonacott AJ (1996) J Mol Biol 21:371–383
31. Bondi A (1964) J Phys Chem 68:441–451
32 Nägele G, Klein R, Medina-Noyola M (1985) J Chem Phys 83:2560–2568
33. Bendedouch D, Chen SH, Koehler WC (1983) J Phys Chem 87:2621–2628
34. Missel PJ, Mazer NA, Benedek GB, Young CY, Carey MC (1980) J Phys Chem 84 1044 1057